Supplementary Information: "Effect of cationic order-disorder on the transport properties of $LaBaCo_2O_{6-\delta}$ and $La_{0.5}Ba_{0.5}CoO_{3-\delta}$ perovskites."

In this document we have included complementary information about the manuscript "**Effect of cationic order-disorder on the transport properties of $LaBaCo_2O_{6-\delta}$ and $La_{0.5}Ba_{0.5}CoO_{3-\delta}$ perovskites**". Some of this information has been also included in the body of manuscript because it is relevant and improves the discussion.

1. Structural Refinement

The structural data used as initial structures in refinements for $La_{0.5}Ba_{0.5}CoO_{3-\delta}$ and $LaBaCo_2O_{6-\delta}$ are listed in Table S1. The selection of both structures is supported for the difference in reflection peaks. Complete NPD-patterns are included in the manuscript. In this document, Figure S1 shows the XRD-pattern between 20 and 70 ° and Figure S2 shows the NPD-pattern between 106-112°. Both figures show the splitting of some (hkl) Bragg reflections corresponding to $La_{0.5}Ba_{0.5}CoO_{3-\delta}$ phase in two peaks for $LaBaCo_2O_{6-\delta}$ supporting the structural difference between both compounds.

The "Experimental" section of manuscript indicates that the NPD and XRD data were refined by Rietveld Method using Fullprof suite tools. During the refinements, a Thompson-Cox-Hastings (TCH) pseudo-Voigt function was used for the peak shape (Thompson et al. 1987). The background of the NPD data obtained at room temperature was refined with a Chebychev polynomial and a linear interpolation of N selected points was used for the data collected at T = 400 °C. A calibration pattern and function were used to separate the size and strain effects in diffraction patterns. Different approaches were used to fit the diffraction peak profiles. These approaches are discussed below:

1. Microstrain effect: The diffraction profiles would be affected by microstructural strain due to the presence of a high concentration of lattice defects in these samples. Thus, a local distortion might appear due to the fact that La^{+3} and Ba^{+2} would not be perfectly random or layered distributed in $La_{0.5}Ba_{0.5}CoO_{3-\delta}$ and $LaBaCo_2O_{6-\delta}$, respectively. Besides, oxygen vacancies might not be randomly distributed, also contributing to microstrain effect. Both effects change locally the lattice parameters broadening the peaks. Two different approaches have been used to model this effect: the integral breadth method (named **Integral**) and the anisotropic strain broadening method (named **Anisotropic**) (Rodríguez-Carvajal 2000). For the latter, the phenomenological description proposed by Stephens in 1999 was applied considering the symmetry of compounds.

2. Debye-Waller factor: The Debye Waller, B-factors or U-factors are indicators of the relative vibrational motion of different parts of the structure. Two approaches have been used, **Isotropic** or **Anisotropic** vibration. For the latter, a phenomenological effect of symmetry was also considered. The anisotropic effect must be more important for the tetragonal symmetry.
3. Oxygen content: Neutron scattering, being more sensitive than X-rays to the oxygen atom, allows obtaining information about their location and occupancy (g_O). Therefore two independent approaches have been used: g_O as a parameter to be fitted (O content **Fit**) and g_O as a parameter to be fitted constraining the overall oxygen content determined by thermogravimetry (O content **Fix**). The chance that oxygen vacancy might be located in different O sites was also evaluated in those cases where the structure presents more than one O-crystallographic site. However, only realistic results were found for O-vacancies located in O2 and O3 sites of $LaBaCo_2O_{6-\delta}$. In other cases, g_O higher that 100% were found.

Table S2 shows the goodness-of-*fit* obtained for each combination of approaches. Three agreement factors are shown: the Reduced chi-square (Chi2), the Profile Factor (Rp) and the Weighted Profile Factor (Rwp). The results of combining the NPD and XRD profile fitting are also shown in this Table. In case that none microstructural or vibrational effects were considered, the profiles fitting gave poor results for adjusting peak width and intensities (these results are not shown here). The goodness of fits for $LaBaCo_2O_{6-\delta}$ and $La_{0.5}Ba_{0.5}CoO_{3-\delta}$ were improved considering **Anisotropic** Stephens microstrain model. For $LaBaCo_2O_{6-\delta}$, a slight improvement was also found after to include **Anisotropic** Debye-Waller coefficient. Despite the fact that the addition of **Anisotropic** Debye Waller coefficients should improve the agreement factors, it was not the case for $La_{0.5}Ba_{0.5}CoO_{3-\delta}$ compound. However, this behavior is reasonably considering the cubic symmetry of this compound.

Finally, the O-content **Fix** approach was also used. Table 3 shows the Anisotropic Atomic Displacement Parameters (U_{11}, U_{22}, U_{33}), and/or the equivalent isotropic displacement parameters (U_{equiv} and B_{iso}) for $LaBaCo_2O_{6-\delta}$ and $La_{0.5}Ba_{0.5}CoO_{3-\delta}$ obtained by fitting the oxygen content (FIT) or by fixing with TG data (FIX). In both cases the anisotropic strain model have been considered. Despite that the refinement at room temperature was not improve by fixing the O content with TG data, we decided to keep this approximation at both temperatures because the atomic thermal displacement shown correlation with the O-content. In addition, it could be seen that the atomic displacement of O3 site is lower than those of other O sites in $LaBaCo_2O_{6-\delta}$ regardless the approximation used.

2. Fourier Analysis

Fourier Maps calculated from NPD and XRD were used to discuss the O-diffusion path and electron-hole transport, respectively. These Fourier maps were built by using observed structure factors (Fobs) and calculated phases from Rietveld method. In this Supplementary Information, we include only the Fourier maps obtained from NPD. Some of these maps and those corresponding to XRD were included in the manuscript supporting the discussion of the transport properties.

Figure S3 and S4 shows the Fourier Maps obtained from NPD for $La_{0.5}Ba_{0.5}CoO_{3-\delta}$ and $LaBaCo_2O_{6-\delta}$ compounds, respectively. The bound coherent scattering lengths (b) for atoms in these structures are b_O = 5.8 fm, b_{Co} =2.4 fm, b_{Ba} = 5.07 fm and b_{La} = 8.24 fm. Therefore, NPD is a powerful technique to obtain information about O sub-lattice in these perovskites.

$La_{0.5}Ba_{0.5}CoO_{3-\delta}$ compound shows an isotropic Fourier map. Figure S3 shows (h00)-plane cutting four unit cells, but this plane is symmetrical equivalent to the (0k0) and (00l) planes. Therefore, a three-dimension (3D) O-migration path might be proposed for this compound.

At difference to that observed for $La_{0.5}Ba_{0.5}CoO_{3-\delta}$, the Fourier maps for $LaBaCo_2O_{6-\delta}$ show an anisotropic behaviour along c-direction. Figure S4 shows the (00l)-planes (a, b, c, f, g, h) and (h00)-planes cutting in different layers. Whereas in (00l) planes the Fobs distribution is isotropic, in (h00) (or (0k0)) planes, the O-density is concentrate thought the LaO layer. Then, the Fourier maps suggest that the O-migration path involves only the O2 and O3 sites.

References

Thompson, P., Cox, D.E., Hastings, J.B. (1987) J. Appl. Cryst **20**, 79–83.

Rodríguez-Carvajal, J. (2000). Fullprof 2000: A program for Rietveld Refinement and Profile Matching Analysis of Complex Powder Diffraction Patterns; Laboratoire Léon Brillouin (CEA-CNRS).

Stephens, P. W. (1999) J. Appl. Cryst. **32**, 281-289

Table S1. Initial structural data used for refinement of $La_{0.5}Ba_{0.5}CoO_{3-\delta}$ and $LaBaCo_2O_{6-\delta}$ phases.

	$La_{0.5}Ba_{0.5}CoO_{3-\delta}$	**$LaBaCo_2O_{6-\delta}$**
Space Group	Pm-3m	P4/mmm
Lattice parameter	a = b = c = 3.8863	a = b = 3.8997, c = 7.7158
Atom positions	(La,Ba) (0,0,0) Co (1/2,1/2,1/2) O (1/2,1/2,0)	La (0,0,1/2) Ba (0, 0, 0) Co (1/2,1/2,0.254) O1 (1/2,1/2,0) O2 (1/2,0,0.3) O3 (1/2,1/2,1/2)

Table S2. Agreement factors obtained from different approaches used during NPD and XRD profiles fit.

	T	Data	Strain	Debye-Waller Factor	O content	Chi2	Rp	Rwp
$La_{0.5}Ba_{0.5}CoO_{3-\delta}$	20ºC	NPD	Integral	Isotropic	Fit	2.90	14.1	11.0
			Anisotropic			2.85	14.0	11.0
				Anisotropic		3.68	15.3	12.4
		NPD		Isotropic	Fix	4.49	16.1	13.7
		XRD				12.3	12.4	14.3
	400ºC	NPD	Integral	Isotropic	Fit	1.75	19.9	11.7
			Anisotropic			1.73	19.9	11.6
				Anisotropic		1.97	20.8	12.3
				Isotropic	Fix	1.73	19.9	11.6
$LaBaCo_2O_{6-\delta}$	20ºC	NPD	Integral	Isotropic	Fit	8.00	18.8	16.7
			Anisotropic			5.11	15.1	13.3
				Anisotropic		4.66	14.4	12.7
		NPD			Fix	5.09	15.7	13.3
		XRD				5.32	10.0	12.6
	400ºC	NPD	Integral	Isotropic	Fit	3.96	20.1	14.5
			Anisotropic			2.95	17.7	12.3
				Anisotropic		2.79	17.2	11.9
					Fix	2.80	17.2	12.0

Table S3. Anisotropic Atomic Displacement Parameters (U_{11}, U_{22}, U_{33}, $U_{12} = U_{13} = U_{23} = 0$), equivalent isotropic displacement parameters (U_{equiv} and B_{iso}), O occupancy (g_O) for $La_{0.5}Ba_{0.5}CoO_{3-\delta}$ and $LaBaCo_2O_{6-\delta}$ obtained considering the oxygen content fitted (FIT) or fixed by TG (FIX).

$La_{0.5}Ba_{0.5}CoO_{3-\delta}$					
20 °C	O FIX by TG, 3-δ = 2.91 (1)				
		B_{iso} (Å^2)			
	O	1.39 (4)			
	O-FIT, 3-δ = 2.95 (2). 54% correlation between Biso and O occupation.				
		B_{iso} (Å^2)			
	O	1.39 (2)			
400 °C	O-FIX by TG, 3-δ = 2.88 (1)				
		B_{iso} (Å^2)			
	O	1.98 (3)			
	O-FIT 3-δ = 2.96 (2). 53% correlation between Biso and O occupation.				
		B_{iso} (Å^2)			
	O	2.04 (3)			
$LaBaCo_2O_{6-\delta}$					
20 °C	O FIX by TG, 6-δ = 5.77 (1)				
		U_{11}x10^2 (Å^2)	U_{22} x10^2 (Å^2)	U_{33} x10^2 (Å^2)	U_{equiv} x10^2 (Å^2)	B_{iso} (Å^2)
	O1	1.3 (3)		0.65 (4)	0. 95	0.75
	O2	0.34 (2)	0.92 (2)	2.13 (6)	1.13	0.89
	O3	0.21(3)		0.07 (1)	0.16	0.13
	g_{O3} =0.80(1), 6-δ = 5.80 (1). 59 % correlation between U33 and O3 occupation.					
		U_{11} x10^2 (Å^2)	U_{22} x10^2 (Å^2)	U_{33} x10^2 (Å^2)	U_{equiv} x10^2 (Å^2)	B_{iso} (Å^2)
	O1	1.2 (1)		0.6 (2)	0.99	0.78
	O2	0.6 (1)	0.78 (1)	2.12 (5)	1.16	0.92
	O3	0.0		0.63 (3)	0.21	0.17
	g_{O2} = 0.99 (1), g_{O3} = 0.80 (1), 6-δ = 5.76 (1). 60 % correlation between U33 and O3 occupation					
		U_{11} x10^2 (Å^2)	U_{22} x10^2 (Å^2)	U_{33} x10^2 (Å^2)	U_{equiv} x10^2 (Å^2)	B_{iso} (Å^2)
	O1	1.2 (1)		0.6 (1)	1.01	0.82
	O2	0.6 (2)	0.7 (4)	2.1 (1)	1.10	0.89
	O3	0.0		0.7 (1)	0.23	0.18
400 °C	O-FIX by TG, 6-δ = 5.71(1)					
		U_{11} x10^2 (Å^2)	U_{22} x10^2 (Å^2)	U_{33} x10^2 (Å^2)	U_{equiv} x10^2 (Å^2)	B_{iso} (Å^2)
	O1	2.6 (3)		0.8 (2)	2.02	1.60
	O2	1.9 (2)	1.2 (1)	3.46 (3)	2.22	1.75
	O3	0.7 (2)		0.7 (3)	0.70	0.55
	g_{O3} = 0.75 (1), 6-δ= 5.75 (1). Correlation lower than 30% between U33 and O3 occupation was found.					
		U_{11} x10^2 (Å^2)	U_{22} x10^2 (Å^2)	U_{33} x10^2 (Å^2)	U_{equiv} x10^2 (Å^2)	B_{iso} (Å^2)
	O1	2.6 (3)		0.70 (2)	1.97	1.56
	O2	1.9 (2)	1.2 (2)	3.41 (4)	2.21	1.74
	O3	1.0 (2)		1.2 (6)	1.06	0.83
	g_{O2} = 0.98 (1), g_{O3} = 0.76 (1), 6-δ= 5.68 (1). Correlation lower than 30% between U33 and O3 occupation was found.					
		U_{11} x10^2 (Å^2)	U_{22} x10^2 (Å^2)	U_{33} x10^2 (Å^2)	U_{equiv}x10^2 (Å^2)	B_{iso} (Å^2)
	O1	2.6 (3)		0.7 (2)	2.01	1.58
	O2	1.9 (2)	1.2 (1)	3.3 (7)	2.14	1.69
	O3	1.0 (3)		1.3 (4)	1.12	0.89
	g_{O2} = 1.01 (1), g_{O3} = 0.76 (1), 6-δ= 5.71 (1).					

	U_{11} x10^2 (Å^2)	U_{22} x10^2 (Å^2)	U_{33} x10^2 (Å^2)	U_{equiv} x10^2 (Å^2)	B_{iso} (Å^2)
O1	2.7 (3)		0.7 (2)	2.01	1.58
O2	1.9 (2)	1.2 (1)	3.3 (7)	2.14	1.69
O3	1.0 (3)		1.29 (6)	1.12	0.88

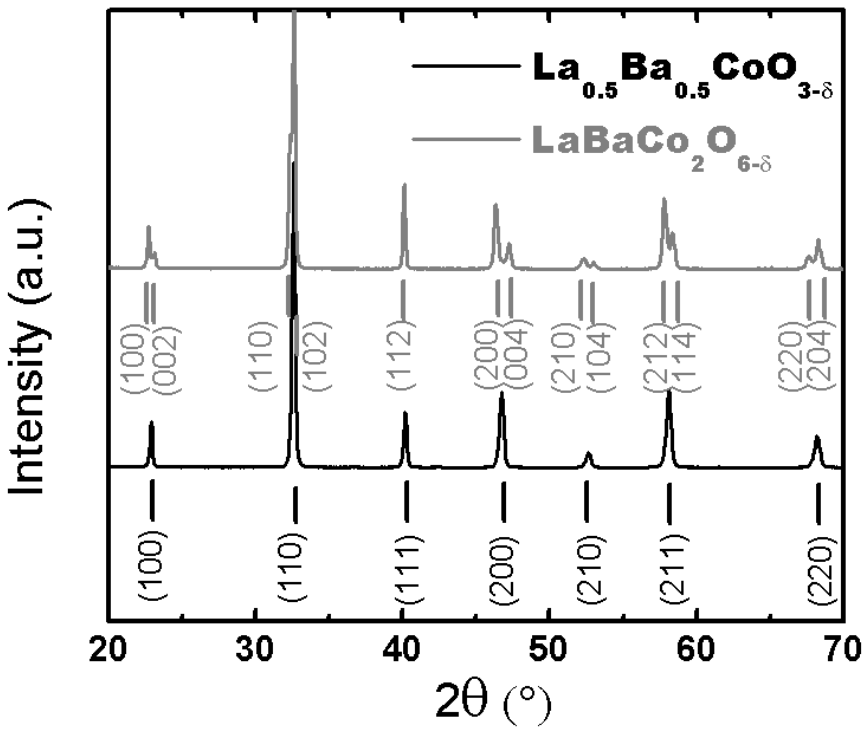

Figure S1. XRD patterns and Bragg reflections between 20-70 ° at 20 °C for $La_{0.5}Ba_{0.5}CoO_{3-\delta}$ and $LaBaCo_2O_{6-\delta}$.

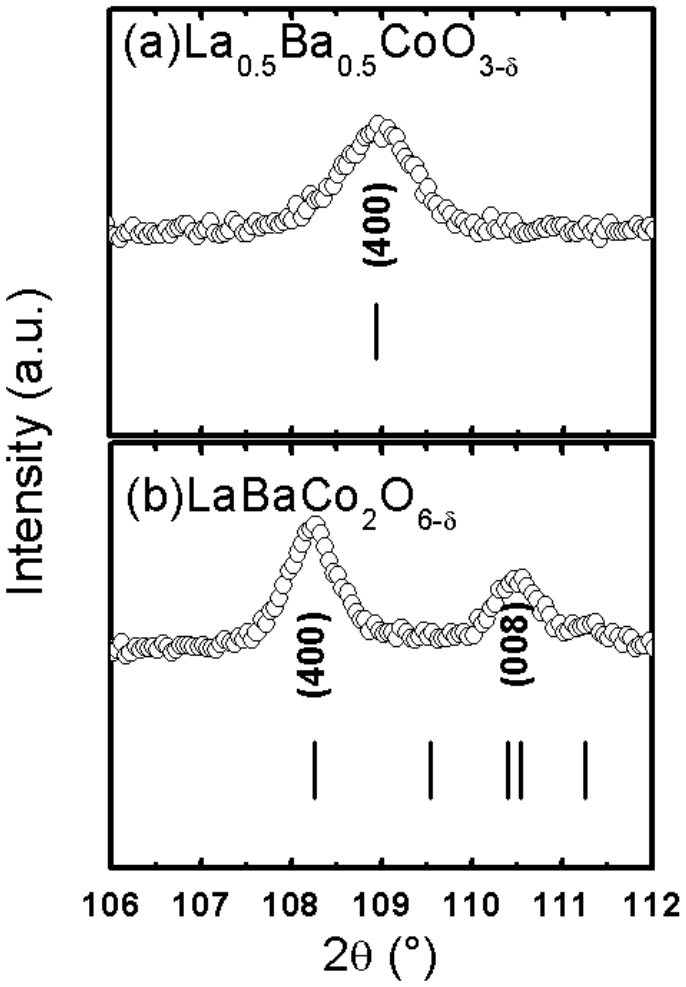

Figure S2. NPD pattern and Bragg reflections between 106-112 ° at 20 °C. (a) $La_{0.5}Ba_{0.5}CoO_{3-\delta}$ and (b) $LaBaCo_2O_{6-\delta}$.

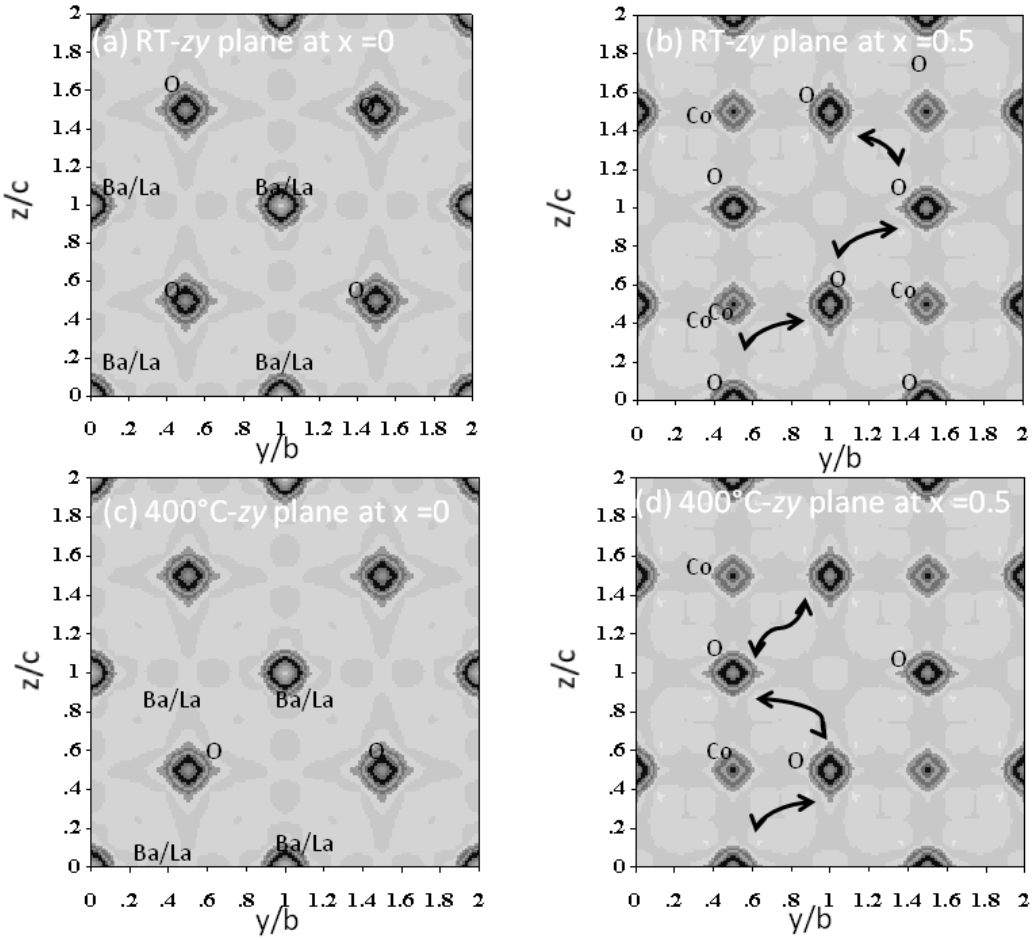

Figure S3. NPD Fourier maps for $La_{0.5}Ba_{0.5}CoO_{3-\delta}$ at room temperature (RT) and 400 °C. (a) and (c) (La,Ba)-O layer corresponding to (100)-plane; (b) and (d) Co-O layer corresponding to (200)-plane. A possible O-migration path is indicated with arrows.

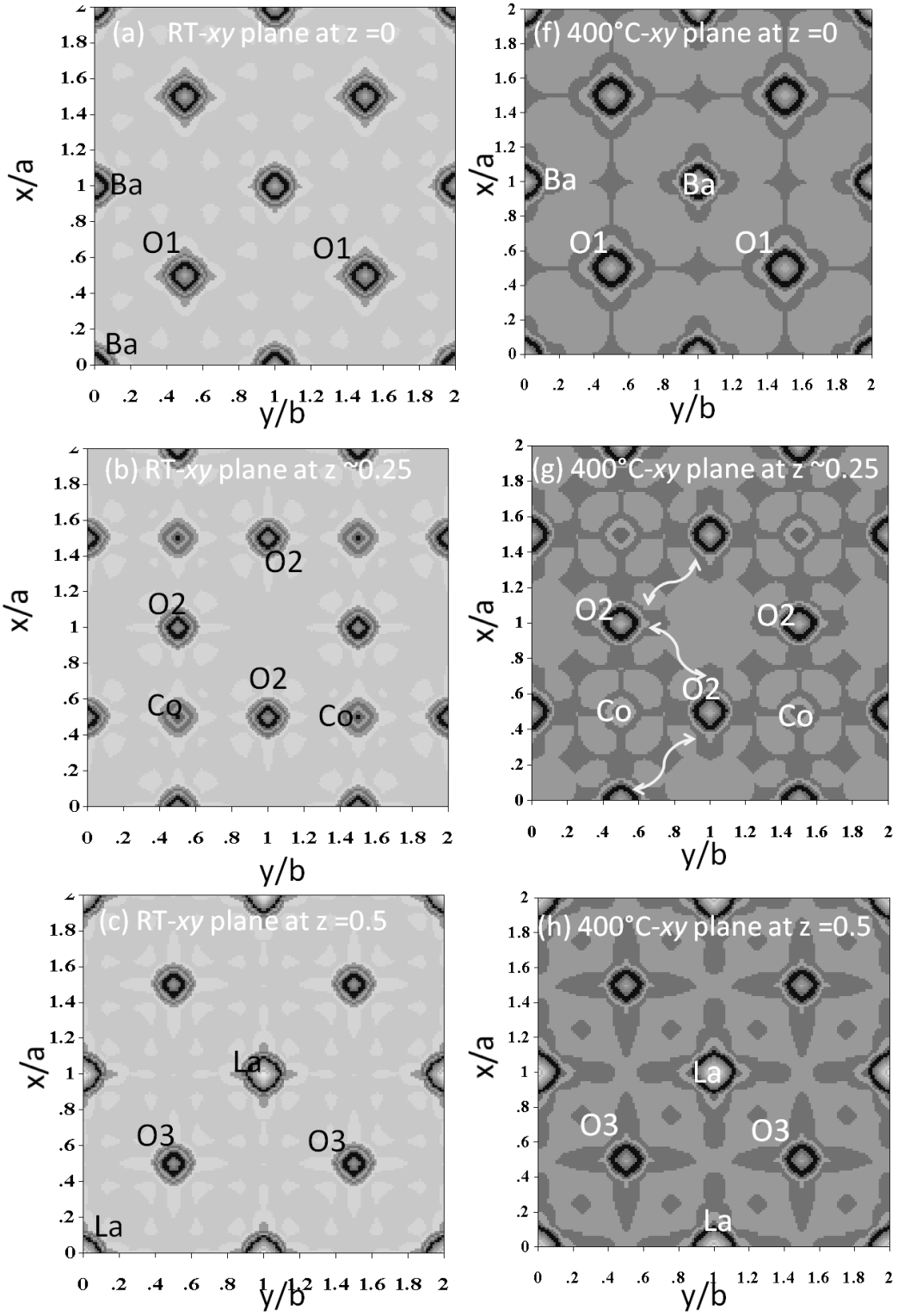

Figure S4. NPD Fourier maps for $LaBaCo_2O_{6-\delta}$ at room temperature (RT) and 400 °C. (a) RT and (f) 400 °C Ba-O layer corresponding to (001)-plane; (b) RT and (g) 400 °C Co-O2 layer corresponding approximately to (004)-plane; (c) RT and (h) 400 °C La-O layer corresponding to (002)-plane; (d) RT and (i) 400°C Ba-O2-La layers corresponding to (100) and/or (010) planes; (e) RT and (j) 400 °C Co-O plane corresponding to (200) and/or (020) planes. Possible O-migration path are indicated with arrows.

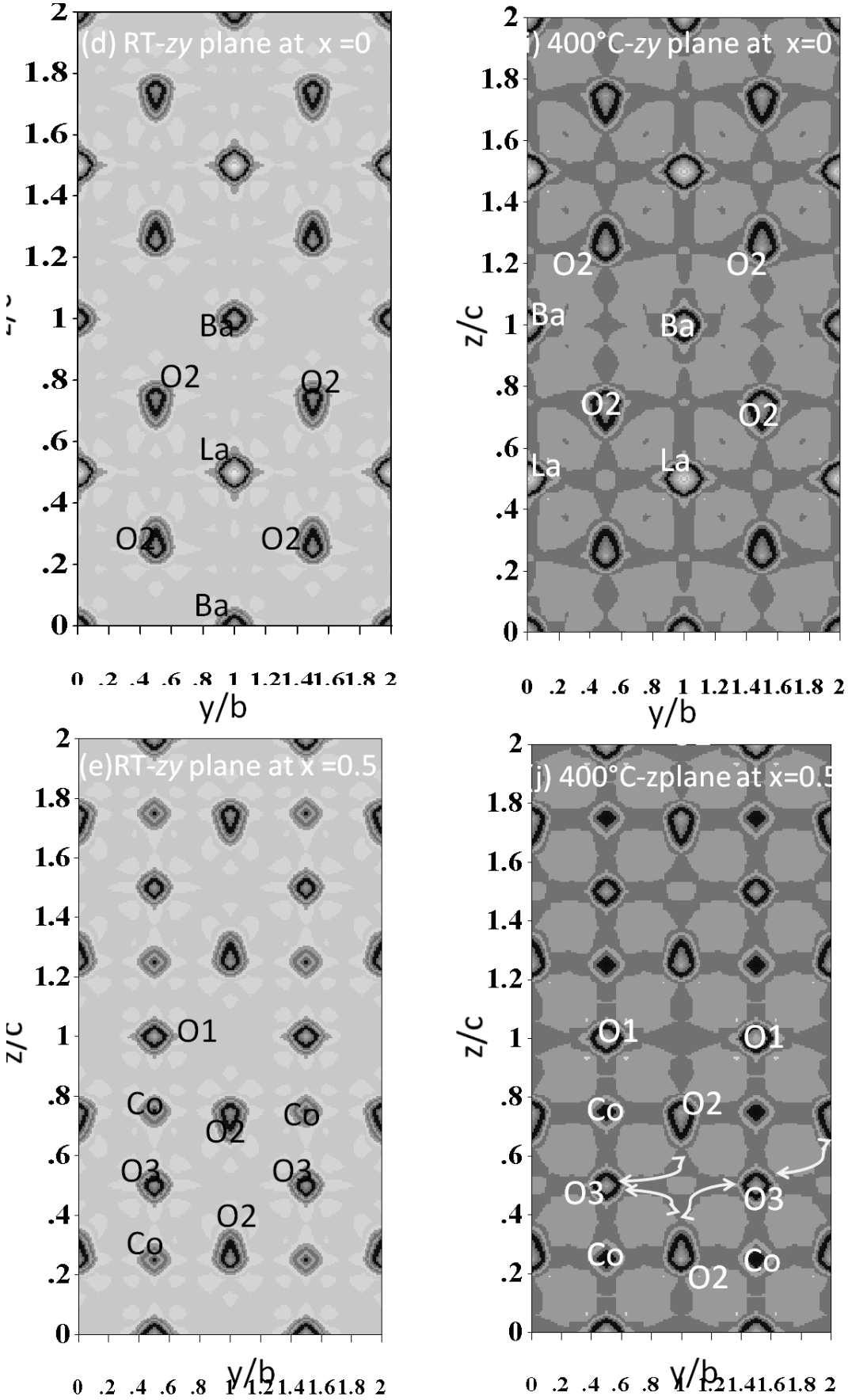

Continue **Figure S4.**